Realization of an Excited, Strongly Correlated Quantum Gas Phase

Elmar Haller, *et al.*

Science **325**, 1224 (2009);
DOI: 10.1126/science.1175850

Realization of an Excited, Strongly Correlated Quantum Gas Phase

Elmar Haller,[1] Mattias Gustavsson,[1] Manfred J. Mark,[1] Johann G. Danzl,[1] Russell Hart,[1] Guido Pupillo,[2,3] Hanns-Christoph Nägerl[1]*

Ultracold atomic physics offers myriad possibilities to study strongly correlated many-body systems in lower dimensions. Typically, only ground-state phases are accessible. Using a tunable quantum gas of bosonic cesium atoms, we realized and controlled in one-dimensional geometry a highly excited quantum phase that is stabilized in the presence of attractive interactions by maintaining and strengthening quantum correlations across a confinement-induced resonance. We diagnosed the crossover from repulsive to attractive interactions in terms of the stiffness and energy of the system. Our results open up the experimental study of metastable, excited, many-body phases with strong correlations and their dynamical properties.

In many-body quantum physics, the interplay between strong interactions and confinement to a low-dimensional geometry amplifies the effects of quantum fluctuations and correlations. A remarkable example in one dimension is the Tonks-Girardeau (TG) gas, in which bosons with strong repulsive interactions minimize their interaction energy by avoiding spatial overlap and acquire fermionic properties (*1*, *2*). Evidence for this ground-state phase was found using Bose-Einstein condensates (BECs) loaded into optical lattices (*3*, *4*). Although many-body quantum systems are usually found in their ground-state phases, long-lived excited-state phases are responsible for some of the most striking physical effects; examples range from vortex lattices in superfluids to subtle topological excitations in spin liquids (*5*). However, the experimental realization of excited phases is difficult because these usually quickly decay from intrinsic effects or by coupling to the environment. In this context, cold atoms (*3*, *4*, *6*–*12*) may provide opportunities for the realization of long-lived, strongly interacting, excited many-body phases because of the excellent decoupling from the environment and the tunability of interactions via, for example, Feshbach resonances (FRs).

For an ultracold one-dimensional (1D) system of bosons, we prepared a highly excited many-body phase known as the super–Tonks-Girardeau (sTG) gas (*13*). In this highly correlated quantum phase, interactions are attractive, and rapid decay into a cluster-type ground state is possible, in principle. However, a surprising property of this many-body phase is its metastability. Attractive interactions strengthen correlations between particle positions and ensure, similar to an effective long-range repulsive interaction, that particles rarely come together. To realize this exotic phase, we observed and exploited a 1D confinement-induced resonance (CIR) (*14*, *15*). This resonance allows us to first enter deeply into the repulsive TG regime in order to establish strong particle correlations and then to switch interactions from strongly repulsive to strongly attractive. The frequency ratio of the two lowest-energy collective modes (*16*) provides accurate diagnostics for the crossover from the TG to the sTG regime. In measuring particle loss and expansion, we studied the time evolution of the system through the crossover.

We tuned the strength of the interaction as characterized by the 3D scattering length a_{3D} by means of a magnetically induced FR (*17*). For a 1D system, a CIR arises and strongly modifies the 1D scattering properties when a_{3D} approaches the harmonic oscillator length $a_\perp = \sqrt{\hbar/(m\omega_\perp)}$ of the transversal confinement with trap frequency $\omega_\perp$ (*14*, *15*). Here, m is the mass of the particles and $\hbar$ is Planck's constant divided by 2π. More precisely, the coupling constant g_{1D} of the 1D δ-function contact potential $U_{1D}(z) = g_{1D}\,\delta(z)$ behaves as (*14*)

$$g_{1D} = -\frac{2\hbar^2}{m a_{1D}} = \frac{2\hbar^2 a_{3D}}{m a_\perp^2}\frac{1}{1 - C\,a_{3D}/a_\perp} \quad (1)$$

where a_{1D} is the 1D scattering length defined by this equation and $C = 1.0326$ is a constant. Thus, the CIR allows tuning of g_{1D}. For values of a_{3D} less than but close to $a_\perp/C$ ($a_{3D} \lesssim a_\perp/C$), the coupling parameter g_{1D} is large and positive, and for $a_{3D} \gtrsim a_\perp/C$ it is large and negative, leading to an effectively attractive interaction. For homogenous systems with $g_{1D} > 0$, it is customary to characterize the strength of interactions by the Lieb-Liniger parameter $\gamma = g_{1D}\,m/(\hbar^2\,n_{1D})$, where n_{1D} is the linear 1D density of the system (*2*, *6*). The TG gas corresponds to the limit $\gamma \gg 1$ or $g_{1D} \to \infty$. As interactions are increased, the system becomes strongly correlated and is fully dominated by its kinetic energy. In previous experiments, without the capability to tune a_{3D}, a maximum of $\gamma \approx 5.5$ was achieved (*4*), whereas an effective strength $\gamma_{eff} \approx 200$ was reached with an additional shallow lattice potential along the longitudinal direction (*3*). In the former experiment, a saturation for the size and energy of the 1D system was observed, and in the latter experiment the momentum distribution was studied.

But what happens in the case of strong attractive interactions $g_{1D} \to -\infty$, that is, $a_{1D} \gtrsim 0$? The ground state for a system of N attractively interacting bosons in 1D is a cluster state (*18*, *19*),

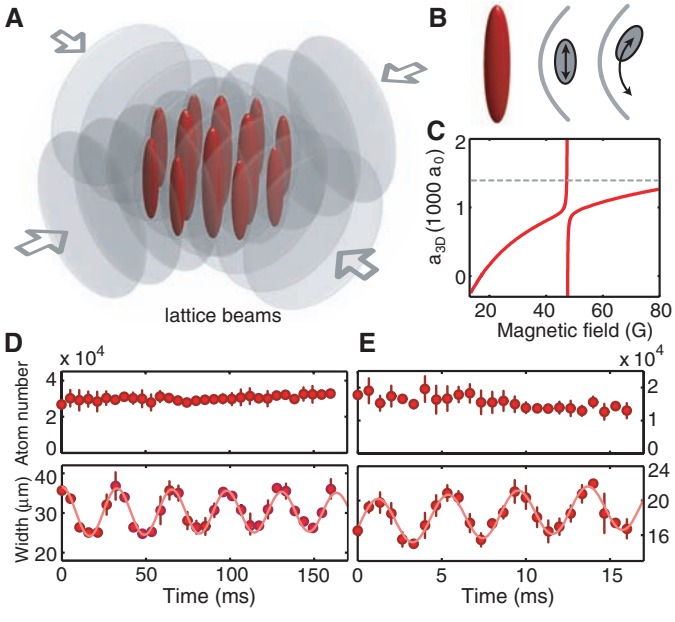

Fig. 1. (**A**) Experimental setup. The lattice potential is created by two retro-reflected laser beams confining the atoms to an array of 1D tubes with equipotential surfaces shown in red. (**B**) Along each tube (left) we excited the lowest compressional mode (center) and compared its frequency to the dipole mode (right). (**C**) The strength of the interatomic interaction is adjusted by tuning the *s*-wave scattering length a_{3D}. The background scattering length rises gently from 0 to 1240 a_0 when the magnetic field B is tuned from 17 to 76 G. Further tuning is possible near a FR at 47.78(1) G to absolute values beyond 4000 a_0. The dashed line indicates $a_\perp/C$ for a transversal trap frequency of $\omega_\perp = 2\pi \times 13.1$ kHz. (**D** and **E**) Typical data sets for the compressional mode in the TG and sTG regimes at $a_{3D} = 875(1)\,a_0$ and $a_{3D} = 2300(200)\,a_0$, respectively. The top panels show the atom number, and the bottom panels show the 1/*e*-cloud-width after time of flight. The solid lines in the bottom panels are sinusoidal fits (*24*), yielding the oscillation frequencies $\omega_C = 2\pi \times 30.6(3)$ Hz and $\omega_C = 2\pi \times 241(1)$ Hz, respectively.

[1]Institut für Experimentalphysik und Zentrum für Quantenphysik, Universität Innsbruck, Technikerstraße 25, A-6020 Innsbruck, Austria. [2]Institut für Theoretische Physik, Universität Innsbruck Technikerstraße 25, A-6020 Innsbruck, Austria. [3]Institut für Quantenoptik und Quanteninformation der Österreichischen Akademie der Wissenschaften, Technikerstraße 21a, A-6020 Innsbruck, Austria.

*To whom correspondence should be addressed. E-mail: christoph.naegerl@uibk.ac.at

which one would expect in a cold-atom system to decay quickly via molecular channels. However, by crossing the CIR from the TG side (switching interactions from $g_{1D} = +\infty$ to $g_{1D} = -\infty$), an excited gaslike phase (the sTG gas) should be accessible (*13*). Is this excited phase stable; does it exist at all? The expectation is that the large kinetic energy inherited from the TG gas, in a Fermi pressure–like manner, prevents the gas from collapsing (*20*). This stability can most simply be inferred from a Bethe-ansatz solution to the Lieb-Liniger model with attractive interactions (*20*, *21*). This ansatz yields for the energy per particle $E/N \approx \hbar^2 \pi^2 n_{1D}^2/[6\, m\, (1 - n_{1D}\, a_{1D})^2]$, corresponding to the energy of a gas of hard rods (*1*), for which a_{1D} represents the excluded volume. This results in a positive inverse compressibility and also in an increased stiffness of the system as long as $n_{1D}\, a_{1D}$ is sufficiently small. In this phase, the density correlations are even stronger than in the TG gas because they show a power-law decay that is slower than for a TG gas (*13*), indicating an effective long-range interaction.

We realized the crossover all the way from a noninteracting gas via the 1D mean-field Thomas-Fermi (TF) regime to a TG gas and then to a sTG gas. We exploited the fact that our 1D systems possess weak harmonic confinement along the axial direction characterized by the confinement length $a_{\|}$. Whereas the frequency ω_D of the lowest dipole mode depends only on the confinement, the frequency ω_C of the lowest axial compressional mode is sensitive to the various regimes of interaction (*16*). For the noninteracting system, one expects $R \equiv \omega_C^2/\omega_D^2 = 4$. This value then changes to $R = 3$ for weakly repulsive interactions in a 1D TF regime (*7*). For increasing positive interaction strength, R is expected to change smoothly to 4 when entering the TG regime as the system becomes fermionized, hence effectively noninteracting. A rise beyond the value of 4, after crossing the CIR, would then constitute clear evidence for the sTG regime (*13*). As a_{1D} is further increased, the system will finally become unstable and R is expected to turn over and drop toward 0. For a harmonically confined system, the point of instability is reached when the overall length of the system of hard rods, $N\, a_{1D}$, becomes of the order of the size $\sqrt{N\, a_{\|}}$ for the wave function of N noninteracting fermions: $A \equiv Na_{1D}/(\sqrt{Na_{\|}}) \approx 1$. We use A^2 as an alternative parameter to γ so as to characterize the strength of the interaction because it accounts for the harmonic confinement.

We started from a 3D BEC with up to 2×10^5 cesium (Cs) atoms with no detectable thermal fraction in a crossed-beam dipole trap with magnetic levitation (*22*). Depending on the interaction regime to be studied, we then set the number of atoms in the BEC to values in the range of 1×10^4 to 4×10^4 by means of forced radio-frequency evaporation. To confine the atoms in 1D (that is, to freeze out transversal motion), we used a 2D optical lattice (*12*), which forms an array of vertically oriented elongated tubes with an aspect ratio that we set to values between 100 and 1000 (Fig. 1A). We occupied between 3000 and 6000 independent tubes with 8 to 25 atoms in the center tube. The interaction strength g_{1D} was controlled by magnetic tuning of a_{3D} by means of a combination of a broad and a narrow FR (Fig. 1C) with poles at $B = -11.1(6)$ G and $B = 47.78(1)$ G and widths of about 29.2 G and 164 mG, respectively (*23*). The broad resonance provides a slow variation of a_{3D}, allowing us to gently tune a_{3D} from 0 a_0 near 17.119 G to about 1240 a_0 near 76 G, whereas the narrow resonance allows us to tune a_{3D} to absolute values beyond 4000 a_0

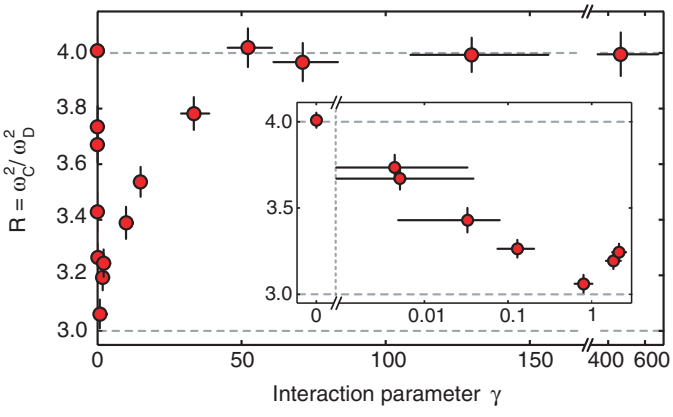

Fig. 2. Transition from the noninteracting regime via the mean-field TF regime into the TG regime. The squared frequency ratio $R = \omega_C^2/\omega_D^2$ of the lowest compressional mode with frequency ω_C and the dipole mode with frequency ω_D serves as an indicator for the different regimes of interaction. For increasing interactions from $\gamma = 0$ to $\gamma \approx 500$, the system passes from the ideal gas regime ($R = 4$) to the 1D TF regime ($R \approx 3$) and then deeply into the TG regime ($R = 4$). The inset shows the transition from the noninteracting regime to the mean-field regime in more detail. The vertical error bars refer to SE and the horizontal error bars reflect the uncertainty in determining a_{1D} and n_{1D} (*24*). The horizontal error bar on the data point at $\gamma = 0$ (not shown in the inset) is ±0.03.

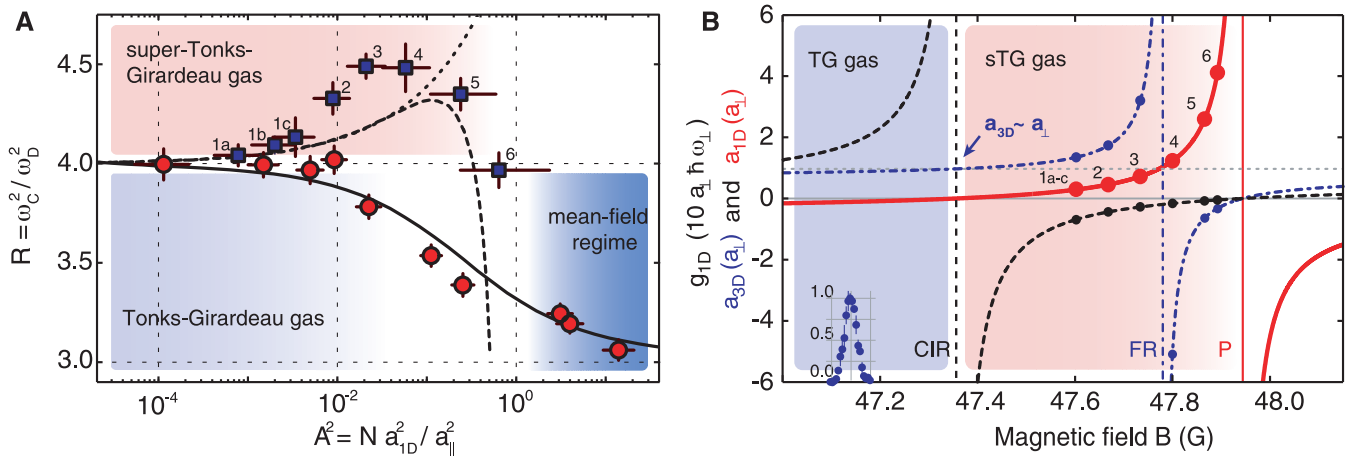

Fig. 3. (**A**) The ratio $R = \omega_C^2/\omega_D^2$ is plotted as a function of the interaction parameter $A^2 = N\, a_{1D}^2/a_{\|}^2$. The squares show the measurements in the attractive regime ($g_{1D} < 0$), providing evidence for the sTG gas. The circles show the transition from the TF to the TG regime ($g_{1D} > 0$; same data as in Fig. 2 for $\gamma > 1$). The solid line presents the theoretical data for $g_{1D} > 0$, and the dashed line presents the theoretical data for $g_{1D} < 0$, by Astrakharchik *et al.* (*13*). The dotted line corresponds to the model of hard rods. For reference, the measurements for $g_{1D} < 0$ are numbered. Data points 1c to 6 are taken at $\omega_D = 2\pi \times 115.6(3)$ Hz. For data points 1a and 1b, the trap frequency is $\omega_D = 2\pi \times 22.4(1)$ Hz and $\omega_D = 2\pi \times 52.3(1)$ Hz, respectively. For all measurements in the sTG regime, $a_{\perp} = 1346(5)\, a_0$. (**B**) The parameters a_{3D} (dashed-dotted), a_{1D} (solid), and g_{1D} (dashed) are plotted in the vicinity of the FR at 47.78(1) G. The horizontal dotted line indicates the value of $a_{\perp}/C$. The pole of the CIR is at 47.36(2) G. a_{1D} has a pole (P) at 47.96(2) G. The bell-shaped curve at the bottom left indicates the atomic distribution as a function of the magnetic field determined from high-resolution microwave spectroscopy.

given our magnetic field control. We converted the applied magnetic field B into a_{3D} using the fit formula of (*23*). A magnetic field gradient, which we used to levitate the atomic sample (*24*), introduced a small spread in the value of a_{3D} across the sample.

To determine the oscillation frequencies ω_C and ω_D of the fundamental modes (Fig. 1B), we excited each mode separately at a given value of the magnetic field B (*24*) and let the atoms evolve for a varying amount of hold time. The distribution was then imaged in momentum space by taking an absorption picture after release and expansion. To avoid possible broadening effects due to interaction during the initial expansion, a_{3D} was set to 0 near B = 17.119 G at the moment of release. To extract the frequency, we determined for each hold time the axial 1/*e*-width of the distribution and then fit a damped sinusoid with linear offset to this data. Typical measurements of ω_C are shown in Fig. 1, D and E. Whereas the atom number remained constant for $g_{1D} > 0$, we observed some atom loss and a slight broadening of the distribution for attractive 1D interactions. In all parameter regimes, the 1D system was sufficiently stable to allow a reliable measurement of ω_C.

We show that we can tune the system from the noninteracting regime deeply into the repulsive TG regime (Fig. 2). In agreement with expectations, the value for $R = \omega_C^2/\omega_D^2$ first drops from 4 to 3 and then increases back to 4 as γ is tuned by means of the gently varying background scattering length. We found that the TG regime is fully reached for $\gamma > 50$. A further increase to values up to $\gamma \approx 500$ does not lead to changes for R. As a_{3D} approaches $a_\perp$, the divergence of g_{1D} according to Eq. 1 has to be taken into account when determining γ (*24*). Heating of the system can be excluded because we can return to a 3D BEC without significant thermal background when ramping down the lattice potential.

The attractive regime was entered by crossing the CIR on the low-field wing of the 47.78 G FR. Here, a_{1D} is small and positive. The central results of this work are summarized in Fig. 3A and compared with the theoretical work of (*13*). We plot $R = \omega_C^2/\omega_D^2$ as a function of the interaction parameter A^2. For reference, Fig. 3B plots a_{3D}, a_{1D}, and g_{1D} in the vicinity of the FR as a function of the magnetic field B. As the CIR is crossed and A^2 is increased, R rises beyond the value of 4. This provides clear evidence for the sTG regime because $R = 4$ is the maximal value for bosons with repulsive contact interaction. This increase is expected from the model of a gas of hard rods, and our data initially follow the prediction from this model. However, as A^2 is increased R reaches a maximum and then starts to drop. The maximum of about 4.5 is reached for $A^2 \approx 3 \times 10^{-2}$. The existence of the maximum is in qualitative agreement with the results obtained from Monte Carlo simulations (*13*). The theoretical prediction, however, underestimates the measured R. This is probably due to the local density approximation, which may not be applicable to our system with low particle numbers. For comparison, the results from Fig. 2 for $\gamma \geq 1$ are shown. $\gamma \approx 500$ corresponds to small values of $A^2 \approx 10^{-4}$. For this data, at higher particle numbers, there is excellent agreement with the theoretical prediction (Fig. 3, solid line) in the entire crossover from the mean-field regime to the TG regime (*16*).

We studied the stability of the system in the crossover from the TG to the sTG regime and found further evidence for the existence of the CIR by recording particle loss and measuring the axial width of the atomic cloud after release from the tubes. The axial width is a measure for the kinetic energy of the system because interactions are instantly switched off upon release. The conditions used were similar to those used for the measurements on the sTG regime presented in Fig. 3. The TG regime was entered adiabatically so as to avoid the excitation of collective modes. The system was prepared at a_{3D} = 887(1) a_0 at a magnetic field of B = 42.77(2) G with about 11 atoms in the central tube. The magnetic field was then ramped to a specific value within 0.2 ms, and the sample was held at this value for a variable hold time τ from 10 to 200 ms. $a_\perp$ was set to 1523(6) a_0. The results (Fig. 4) for different hold times τ in the tubes show that for τ = 10 ms, corresponding to the timescale of the measurements in the sTG regime shown in Fig. 3, the transition from the TG to the sTG regime appears very smooth. There is essentially no particle loss when the system is deep in the TG regime and close to the CIR. The loss gradually increases in the attractive regime as one moves to larger values of B and toward the pole for a_{1D}. Correspondingly, the width of the sample exhibits a smooth behavior across the CIR, showing a slight increase for larger B. This behavior is consistent with the expectation of an increased energy in the sTG regime (*13*).

For longer hold times, the data for the atom number and the sample width develop distinct features at the calculated position of the CIR. Evidently, the system is in a transient state. For τ = 50 ms, the number of remaining atoms shows a dip that correlates with a peak in the kinetic energy of the sample. Both features become more prominent and asymmetric for longer hold times (τ = 100 and 200 ms). In comparison, no pronounced effects are visible at the pole of the FR for a_{3D}. Our results must be connected to the fact that the energy spectrum of the system changes dramatically across the CIR, from the TG to the sTG regime (*19*). The system acquires a deeply lying ground state together with a family of lower lying many-body excited states, potentially opening up new decay channels. Also, the CIR strongly modifies the two-body scattering problem, making formation of confinement-induced molecules in transversally excited trap states (*14*) possible.

The nontrivial time evolution observed in this system raises intriguing questions on possible coupling and decay mechanisms for strongly interacting, excited, many-body systems, in particular in the context of integrability of 1D systems (*25*). Our results offer an example of the counterintuitive effects that occur in many-body systems and open up the possibility to study the dynamical properties of strongly correlated systems with effective long-range interactions (*26*, *27*) under conditions in which all parameters are tunable and, in fact, can be changed dynamically. Similar to magnetic FRs in atomic scattering, we expect the confinement-induced resonance demonstrated here to serve as

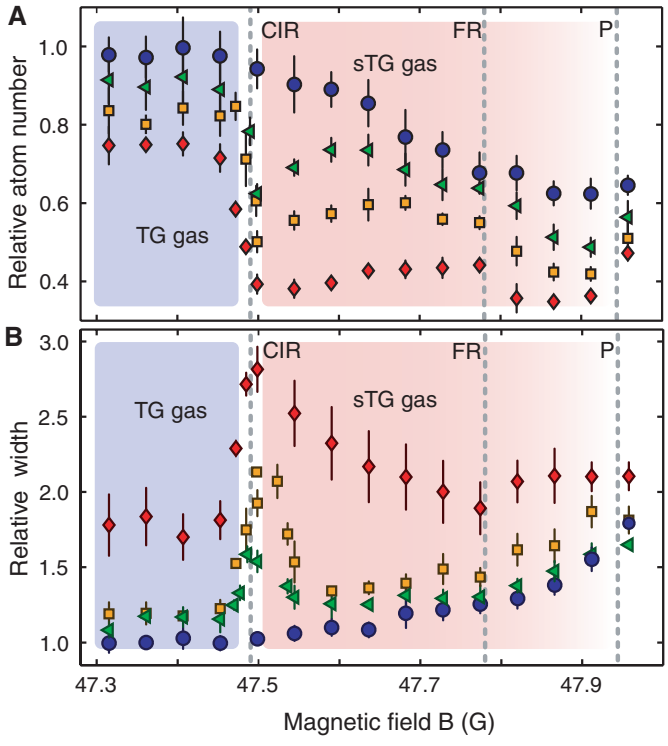

Fig. 4. Stability and kinetic energy in the TG and sTG regimes. **(A)** Relative number of atoms remaining and **(B)** relative 1/*e*-width along the axial direction after 10 ms expansion, after a hold time τ = 10, 50, 100, and 200 ms (circles, triangles, squares, and diamonds, respectively) at a given magnetic field B. The position of the CIR, the pole of the FR, and the pole for a_{1D} (P) are as indicated. For these measurements, $a_\perp$ = 1523(6) a_0 and $\omega_D = 2\pi \times 115.6(3)$ Hz. The atom number is normalized to the initial value of $1.7(1) \times 10^4$, and the width is normalized to the initial value in the TG regime.

a general tool to tailor interactions in 1D and possibly also in 2D systems (*28*), allowing for the further investigation of strongly correlated phases in the context of cold atomic gases.

References and Notes

1. M. Girardeau, *J. Math. Phys.* **1**, 516 (1960).
2. E. H. Lieb, W. Liniger, *Phys. Rev.* **130**, 1605 (1963).
3. B. Paredes *et al.*, *Nature* **429**, 277 (2004).
4. T. Kinoshita, T. Wenger, D. S. Weiss, *Science* **305**, 1125 (2004).
5. F. Alet, A. M. Walczak, M. P. A. Fisher, *Physica A* **369**, 122 (2006).
6. D. S. Petrov, G. V. Shlyapnikov, J. T. M. Walraven, *Phys. Rev. Lett.* **85**, 3745 (2000).
7. H. Moritz, T. Stöferle, M. Köhl, T. Esslinger, *Phys. Rev. Lett.* **91**, 250402 (2003).
8. B. L. Tolra *et al.*, *Phys. Rev. Lett.* **92**, 190401 (2004).
9. D. S. Petrov, D. M. Gangardt, G. V. Shlyapnikov, *J. Phys. IV France* **116**, 3 (2004).
10. S. Hofferberth, I. Lesanovsky, B. Fischer, T. Schumm, J. Schmiedmayer, *Nature* **449**, 324 (2007).
11. N. Syassen *et al.*, *Science* **320**, 1329 (2008).
12. I. Bloch, J. Dalibard, W. Zwerger, *Rev. Mod. Phys.* **80**, 885 (2008).
13. G. E. Astrakharchik, J. Boronat, J. Casulleras, S. Giorgini, *Phys. Rev. Lett.* **95**, 190407 (2005).
14. T. Bergeman, M. G. Moore, M. Olshanii, *Phys. Rev. Lett.* **91**, 163201 (2003).
15. M. Olshanii, *Phys. Rev. Lett.* **81**, 938 (1998).
16. C. Menotti, S. Stringari, *Phys. Rev. A* **66**, 043610 (2002).
17. S. Inouye *et al.*, *Nature* **392**, 151 (1998).
18. J. B. McGuire, *J. Math. Phys.* **6**, 432 (1965).
19. E. Tempfli, S. Zöllner, P. Schmelcher, *N.J. Phys.* **10**, 103021 (2008).
20. M. T. Batchelor, M. Bortz, X. W. Guan, N. Oelkers, *J. Stat. Mech.* **10**, L10001 (2005).
21. G. E. Astrakharchik, D. Blume, S. Giorgini, B. E. Granger, *Phys. Rev. Lett.* **92**, 030402 (2004).
22. T. Weber, J. Herbig, M. Mark, H.-C. Nägerl, R. Grimm, *Science* **299**, 232 (2003).
23. A. D. Lange *et al.*, *Phys. Rev. A* **79**, 013622 (2009).
24. Material and methods are available as supporting material on *Science* Online.
25. T. Kinoshita, T. Wenger, D. S. Weiss, *Nature* **440**, 900 (2006).
26. M. Bockrath *et al.*, *Nature* **397**, 598 (1999).
27. H. Steinberg *et al.*, *Nat. Phys.* **4**, 116 (2008).
28. D. S. Petrov, M. Holzmann, G. V. Shlyapnikov, *Phys. Rev. Lett.* **84**, 2551 (2000).

29. We thank S. Giorgini and C. Menotti for helpful discussions and for providing the theory curves shown in Fig. 3A. We are indebted to R. Grimm for generous support and to H. Häffner and his group for the loan of a charge-coupled device camera. We gratefully acknowledge funding by the Austrian Ministry of Science and Research (Bundesministerium für Wissenschaft und Forschung) and the Austrian Science Fund (Fonds zur Förderung der wissenschaftlichen Forschung) in the form of a START prize grant and by the European Union through the Specific Targeted Research Project FP7-ICT-2007-C project NAME-QUAM (Nanodesigning of Atomic and Molecular Quantum Matter) and within the framework of the EuroQUASAR collective research project Quantum-Degenerate Gases for Precision Measurements. R.H. is supported by a Marie Curie International Incoming Fellowship within the 7th European Community Framework Programme.

Supporting Online Material

www.sciencemag.org/cgi/content/full/325/5945/1224/DC1
Materials and Methods
References

4 May 2009; accepted 14 July 2009
10.1126/science.1175850

Complete Methods Set for Scalable Ion Trap Quantum Information Processing

Jonathan P. Home,* David Hanneke, John D. Jost, Jason M. Amini, Dietrich Leibfried, David J. Wineland

Large-scale quantum information processors must be able to transport and maintain quantum information and repeatedly perform logical operations. Here, we show a combination of all of the fundamental elements required to perform scalable quantum computing through the use of qubits stored in the internal states of trapped atomic ions. We quantified the repeatability of a multiple-qubit operation and observed no loss of performance despite qubit transport over macroscopic distances. Key to these results is the use of different pairs of $^{9}Be^{+}$ hyperfine states for robust qubit storage, readout, and gates, and simultaneous trapping of $^{24}Mg^{+}$ "re-cooling" ions along with the qubit ions.

The long-term goal for experimental quantum information processing is to realize a device that involves large numbers of qubits and even larger numbers of logical operations (*1*, *2*). These resource requirements are defined both by the algorithms themselves and the need for quantum error correction, which makes use of many physical systems to store each qubit (*1*, *3*). The required components for building such a device are robust qubit storage, single- and two-qubit logic gates, state initialization, readout, and the ability to transfer quantum information between spatially separated locations in the processor (*2*, *4*, *5*). All of these components must be able to be performed repeatedly in order to realize a large-scale device.

One experimental implementation of quantum information processing uses qubits stored in the internal states of trapped atomic ions. A universal set of quantum logic gates has been demonstrated using laser addressing (*6*–*8*), leading to a number of small-scale demonstrations of quantum information protocols, including teleportation, dense-coding, and a single round of quantum error correction (*6*). A major challenge for this implementation is now to integrate scalable techniques required for large-scale processing.

A possible architecture for a large-scale trapped-ion device involves moving quantum information around the processor by moving the ions themselves, in which the transport is controlled by time-varying potentials applied to electrodes in a multiple-zone trap array (*5*, *9*, *10*). The processor would consist of a large number of processing regions working in parallel, with other regions dedicated to qubit storage (memory). A general prescription for the required operations in a single processing region is the following (Fig. 1), which includes all of the elements necessary for universal quantum computation (*11*): (i) Two qubit ions are held in separate zones, allowing individual addressing for single-qubit gates, state readout, or state initialization. (ii) The ions are then combined in a single zone, and a two-qubit gate is performed. (iii) The ions are separated, and one is moved to another region of the trap array. (iv) A third ion is brought into this processing region from another part of the device. In this work, we

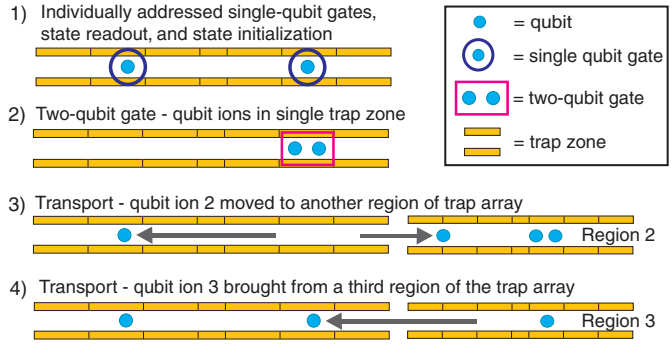

Fig. 1. Schematic of the sequence of operations implemented in a single processing region for building up a computation in the architecture of (*5*, *9*). A large-scale device would involve many of these processing regions performing operations in parallel along with additional regions for memory. Generalized operations would use this block structure repeatedly, with perhaps some of the steps omitted.

Time and Frequency Division, National Institute of Standards and Technology (NIST), Boulder, CO 80305, USA.

*To whom correspondence should be addressed. E-mail: jonathan.home@gmail.com